Boosted Semileptonic Tops in Stop Decays

Tilman Plehn,[1] Michael Spannowsky,[2] and Michihisa Takeuchi[1]

[1]*Institut für Theoretische Physik, Universität Heidelberg, Germany*
[2]*Department of Physics and Institute of Theoretical Science, University of Oregon, Eugene, USA*

Top partner searches are one of the key aspects of new physics analyses at the LHC. We correct an earlier statement that supersymmetric top searches based on decays to semileptonic tops are not promising. Reconstructing the direction of the boosted leptonic top quark and correlating it with the measured missing transverse energy vector allows us to reduce the top pair background to an easily manageable level. In addition, reconstructing the full momentum of the leptonic top quark determines the stop mass based on an M_{T2} endpoint.

Searches for top squarks at hadron colliders aim at a fundamental questions of electroweak symmetry breaking: if the Higgs boson should be a fundamental scalar, how can its mass be stabilized? In particular, is the Higgs mass protected by some symmetry? Such symmetries typically predict the existence of a top partner, like in supersymmetric or little Higgs models [1, 2]. In such a case, studying the properties of top partners allows us to unravel the nature of such an underlying fundamental symmetry protecting the fundamental Higgs mass at the scale of electroweak symmetry breaking.

At the Tevatron, low-mass stop searches look for loop-induced stop decays [3] to charm quarks and the lightest neutralino [4]. Slightly larger stop masses more in agreement with theoretical expectations makes it more promising to look for decays to a bottom jet and the lightest chargino [5]. For leptonic chargino decays this signatures is irreducible from a leptonic top decay. Finally, if the stop becomes heavier and the strong decay in a top quark and a gluino is not yet kinematically allowed, the stop can decay into a top quark and the lightest neutralino [3]. Because it includes on-shell top quarks as stop decay products this channel is the hardest to extract at the LHC. For hadronically decaying top quarks we know that this final state has the advantage that we can fully reconstruct its kinematics, which puts us into a promising position to study angular correlations in the stop pair final state [6]. Extending this analysis strategy to semileptonic stop decays is the aim of this study.

There have been several suggestions as to what we might be able to say about the nature of the stop based on a momentum reconstruction of its visible decay products [7]; the first ingredient to any such analysis is a way to extract stop pairs from the overwhelming top pair background, the second the reconstruction of the stop 4-momentum. Over almost the entire supersymmetric parameter space standard analysis methods fail at both tasks. On the other hand, fully hadronic top pairs we can tag and fully reconstruct using fat jet analysis tools [6, 8, 9]. Using the HEPTopTagger [6, 9] we can extract the stop signature for a wide range of stop masses, reconstruct the top 4-momentum with high precision, and reconstruct the stop mass using a simple M_{T2} endpoint analysis [6]. Obviously, we can use the same strategy for the hadronic side of signatures related to semileptonic top pairs.

The key idea behind the reconstruction of hadronically decaying heavy particles using fat jets is to study the clustering history of a jet algorithm for geometrically large jets including boosted heavy particles. This idea was originally developed for W bosons and top quarks [10, 11] and very successfully applied to Higgs decays to bottoms [12], hadronic top decays [6, 8, 9] as well as supersymmetric particle decays [13].

The obvious question is what we can learn from boosted hadronically decaying top analyses for the equally boosted leptonic top decay [14]. The main shortcoming of the traditional W and top mass constrained reconstruction is that we cannot use the missing transverse momentum vector as a cut against backgrounds after we use it for the reconstruction. The aim is to instead limit ourselves to the particular features of collinear leptonic top decays to reconstruct the top kinematics [15, 16].

In this paper we will proceed in two steps: first, we show how to reconstruct the direction of the top 3-momentum exploiting the typical kinematic features of boosted leptonic top decays. A cut on this top direction serves as the main ingredient to the extraction of semileptonic stop pairs. Second, again using typical features of boosted top decays we reconstruct the full 4-momentum of the top quark. In analogy to hadronically decaying tops this reconstruction could be a starting point to many more phenomenological top pair analyses.

I. SEMILEPTONIC STOP DECAYS

To illustrate the power of reconstructing leptonic top pairs we show how we can extract the stop signature

$$pp \to \tilde{t}_1 \tilde{t}_1^* \to (t\tilde{\chi}_1^0)\,(\bar{t}\tilde{\chi}_1^0) \to (b\ell^+\nu\tilde{\chi}_1^0)\,(\bar{b}jj\tilde{\chi}_1^0) + (bjj\tilde{\chi}_1^0)\,(\bar{b}\ell^-\bar{\nu}\tilde{\chi}_1^0) \tag{1}$$

including missing energy from top decay and from the dark matter agent from top pair production. Our analysis will proceed based on two strategies: first, we suggest a simple approximation of the top decay kinematics to reconstruct the direction of the top 3-momentum (Section II) and the full 4-momentum (Section III). This way we arrive at a two-step strategy to distinguish the stop signal from top pair backgrounds based on the reconstructed top direction and on its reconstructed 4-momentum.

Typical semileptonic analyses start from a set of acceptance cuts requiring at least four jets and a charged lepton [6]. In our case we include a hadronic top tag, which means we require

1. exactly one trigger lepton ($p_T > 20$ GeV, $|\eta| < 2.5$ and isolation $E_T/E_{T,\ell} < 0.1$ within $R = 0.2$)
2. missing transverse momentum $\not{p}_T > 150$ GeV
3. one tagged hadronic top (mass drop, $p_T > 200$ GeV, HEPTopTagger default [6], Fastjet [17])
4. one b tag among the leading 3 jets outside the tagged top (C/A with $R = 0.5$, $p_T > 25$ GeV, $|\eta| < 2.5$)
5. a bottom-lepton invariant mass allowed by the top decay kinematics $m_{b\ell} < \sqrt{m_t^2 - m_W^2} = 154.6$ GeV.

The missing energy cut in combination with the lepton requirement safely removes all QCD backgrounds, including b pair production. In our analysis we do not take into account fakes from pure QCD events.

The main Standard Model background after these first analysis steps is W+jets production, with an inclusive W cross section roughly 200 times the top pair production rate. The probability to fake a tagged top from W+jets events ranges around 4%, after requiring to observe a fat jet with $p_T > 200$ GeV [6]. The tagging efficiency and mis-tagging rate for the HEPTopTagger have to be confirmed by a full experimental study and should in addition be tested on a sufficiently large $t\bar{t}$ sample at the LHC. Including the additional b tag we expect semileptonic $t\bar{t}$ pairs to become the main background to our stop searches. The bottom jet isolation from the top fat jet is defined geometrically. For the b tag we assume a (mis-) tagging probability of $(60\%, 2\%)$ as an event weight factor. Charm jets with a generically higher mis-tagging probability should not spoil our analysis because of their suppression compared to high-multiplicity gluon production.

The status after these first five analysis steps we show in Table I. The stop with different masses we assume to decay with a 100% branching ratio to a top quark and a 98 GeV lightest neutralino. The NLO normalization of the Herwig++ [18] signal sample we obtain from Prospino [19]. The top pair sample from Alpgen-Pythia we normalize to the approximate NNLO rate around 918 pb [20]. For subleading W+jets background we use the default Alpgen-Pythia normalization [21]. For signal and background we include initial and final

	$\tilde{t}_1\tilde{t}_1^*$				$t\bar{t}$	W+jets	S/B	$S/\sqrt{B}_{20\text{fb}^{-1}}$
$m_{\tilde{t}}$[GeV]	340	440	540	640			440	440
0. cross section	5090	1280	402	146	$9.2 \cdot 10^5$	$2.1 \cdot 10^5$	0.001	3.8
1. one lepton	1471	373	118	42.5	$2.6 \cdot 10^5$	$1.3 \cdot 10^5$	0.001	2.7
2. $\not{p}_T > 150$ GeV	569	239	90.2	35.5	9825	4512	0.017	8.9
3. hadronic top tag	74.5	38.0	16.8	7.72	1657	141	0.021	4.0
4′. tagged b jet (100%,0%)	47.2	24.3	11.3	5.22	1057	0.00	0.023	3.3
4. tagged b jet (60%,2%)	31.2	15.9	7.33	3.38	668	4.35	0.024	2.7
5. $m_{b\ell} < m_{b\ell}^{\max}$	27.5	13.7	6.34	2.90	642	2.61	0.021	2.4

Table I: Signal (for different stop masses) and backgrounds for the base analysis. All numbers given in fb. For W+jets, we only show numbers after pre-selection ($n_{\text{jets}} \geq 3$).

state radiation, hadronization and underlying event. The top and stop samples we generate inclusively without restricted decays.

Table I shows how the main analysis steps act on the signal and the dominant backgrounds. Indeed, we see that while the lepton and missing energy requirements are easily passed by all backgrounds, the hadronic top tag and the b tag significantly reduce the W+jets backgrounds and leave us with the dominant top pair contamination. For the hadronic top tag we observe the expected large efficiency for heavier stop samples as compared to continuum $t\bar{t}$ production, which comes from the harder $p_{T,t}$ spectrum.

While these initial results are promising, Table I clearly indicates that we definitely need another set of analysis steps to improve the signal-to-background ratio to a manageable level, to be able to cope with systematic experimental and theoretical uncertainties.

II. RECONSTRUCTING THE TOP DIRECTION

The main difference between the reconstruction of a hadronically decaying top and a leptonic top decays is the significantly smaller number of observables. Aside from the boost of the top and its correlations with other particles in the final state we have to rely on three measurements

$$E_\ell \qquad\qquad E_b \qquad\qquad m_{b\ell}\,, \tag{2}$$

assuming that we know the bottom and lepton 4-vectors after identifying the particles. The invariant mass can be replaced by the angle between the lepton and b momenta.

There have been a few attempts to find strategies to identify boosted tops decaying leptonically. One of them are 'stuck leptons', referring to leptons which are not well isolated from the b jet from the top decay [15, 16]. The invariant mass of the visible top decay products $m_{b\ell}$ is not necessarily close to its upper bound if the neutrino is not observed. Nevertheless, the mass drop $m_b^2/m_{b\ell}^2$ ranges around zero for boosted tops and W+jets while it tends towards one for heavy flavor jets. Because Eq.(2) tells us that there exist three distinctive kinematic observables we can combine the mass drop measurement with preferably sizeable $\Delta R_{b\ell}$ and $E_\ell/(E_\ell+E_b) \sim 0.4$ to construct a leptonic top tagger, but with a limited yield [15]. One strategy to improve the tagging/rejection efficiencies is to include the tracker-level mini-isolation observable $p_{T,\ell}/\sum p_{T,\text{charged}} > 0.9$ summed over all charged tracks within a cone around the lepton or muon [16].

Our strategy is similar to those in the sense that we attempt to reconstruct (parts of) the top 4-momentum without making use of the measured missing transverse energy. This allows us to contrast the top 4-momentum with the measured missing energy vector as a background rejection cut. However, we follow a different path to extract information on the top 4-momentum. To describe the 3-momenta of the top decay products we define the orthonormal coordinate system

$$\begin{aligned}
\hat{p}^\text{D} &= \frac{\vec{p}_{b\ell}}{|\vec{p}_{b\ell}|} && \text{leading } \vec{p}_{b\ell} \text{ direction in } b-\ell \text{ decay plane} \\
\hat{p}^\parallel &= \frac{\vec{p}_\ell - (\vec{p}_\ell \cdot \hat{p}^\text{D})\,\hat{p}^\text{D}}{|\vec{p}_\ell - (\vec{p}_\ell \cdot \hat{p}^\text{D})\,\hat{p}^\text{D}|} && \text{subleading direction in } b-\ell \text{ decay plane} \\
\hat{p}^\perp &= \hat{p}^\text{D} \times \hat{p}^\parallel && \text{subleading direction to } b-\ell \text{ decay plane.}
\end{aligned} \tag{3}$$

Within this coordinate system the neutrino momentum is parameterized as

$$\vec{p}_\nu = x_\text{D}\hat{p}^\text{D} + x_\parallel \hat{p}^\parallel + x_\perp \hat{p}^\perp. \tag{4}$$

In the appendix we show the relative size of these three components.

To reconstruct the neutrino momentum, assuming we know the neutrino mass, we need three components. Because we want to compare the neutrino momentum from the reconstructed top to the measured two-dimensional missing transverse momentum $\not{\vec{p}}_T$ these are three actual unknowns. The W and top mass constraints give us

two, so we need to make at least one assumption to describe the collinear decay of a boosted top. As shown in the appendix, we can choose two well motivated approximations

$$\begin{aligned} x_\perp &= 0 \qquad && \text{decay plane approximation} \\ x_\parallel &= 0 \qquad && \text{orthogonal approximation,} \end{aligned} \tag{5}$$

and correspondingly estimate the neutrino momentum as

$$\bar{p}_\nu^{\text{est}}\Big|_\parallel \qquad \text{or} \qquad \bar{p}_\nu^{\text{est}}\Big|_\perp \,. \tag{6}$$

Based on this estimated neutrino momentum we can construct measurements which distinguish for example the stop signal from the top pair background where the main difference is the existence of additional sources of missing momentum in the signal.

Before constructing such observables we need to sketch a few features of the two approximations for the neutrino and top momentum estimates. For example, the mass constraints are quadratic constraints, so we cannot expect a unique solution for the neutrino and top momenta. Instead, there will be a set of four discrete solutions from which we need to extract the physical solution. The decay plane approximation, which as we will discuss in the appendix is motivated by the Jacobian peak in the top momentum we consistently accept the solution which returns the smallest top momentum. For the orthogonal approximation, which rejects the $t\bar{t}$ background most efficiently, we take the solution which gives the smaller subtracted missing momentum $\not{p}_T - p_{T,\nu}^{\text{est}}$.

Reconstructing the direction of the neutrino 3-momentum or the top 3-momentum is of course not a full reconstruction as we know it from the hadronic top decays using the HEPTopTagger. However, even with its reduced numbers of observables it is sufficient for example to reconstruct the azimuthal angle between the estimated neutrino or top direction and the measured missing transverse energy

$$\Delta\phi \equiv \Delta\phi(\not{\vec{p}}_T, \hat{p}^{\text{est}}) = \phi(\not{\vec{p}}_T) - \phi(\hat{p}^{\text{est}}) \,. \tag{7}$$

The estimated momentum entering this azimuthal difference is not uniquely fixed. We can use the estimated neutrino momentum, the estimated leptonically decaying top momentum, or the momentum of the lepton-bottom system.

From the discussion in the appendix estimating the top direction appears to be more promising than estimating the neutrino direction, simply because the neutrino momentum with its large relative uncertainty constitutes only a small part of the top momentum. In addition, the studies in the appendix suggest to use the orthogonal approximation for this azimuthal angle study. As a starting point we look at the correlations between the measured missing transverse energy vector and the reconstructed leptonic top directions. It turns out that this observable has the best yield for the stop pair search. In the top row of Figure 1 we show the $\Delta\phi$ distributions for the stop signal and the top backgrounds for the orthogonal approximation defined in Eq.(5). It shows a clear difference between signal and $t\bar{t}$ events for all three choices. The signal shows hardly a peak because the reconstructed momentum does not correspond to a physical momentum and is hence uncorrelated. The width of the background peak which we need to cut out is smallest when we include the estimated top direction, as compared to the neutrino or bottom-lepton directions. This includes a hadron level simulation, but the picture might of course change once we include a detector simulation. Qualitatively, all three reconstructed directions work at a similar level.

Improving over this one-dimensional $\Delta\phi$ distribution we can include the correlation with the measured missing transverse momentum. It exploits the following feature: for semileptonic top pair events, if the originating top is not boosted enough, there exists an upper bound for the neutrino momentum. To observe large $\not{p}_T$, the originating top momentum has to be aligned with the $\not{p}_T$ direction. Again, in Figure 1 we show the results for three reconstructed momentum directions, which work qualitatively the same.

These observations we can turn into an analysis strategy to extract semileptonic stop pairs after applying the five generic steps shown in Table I. First of all, it is not guaranteed that given a measured bottom and lepton

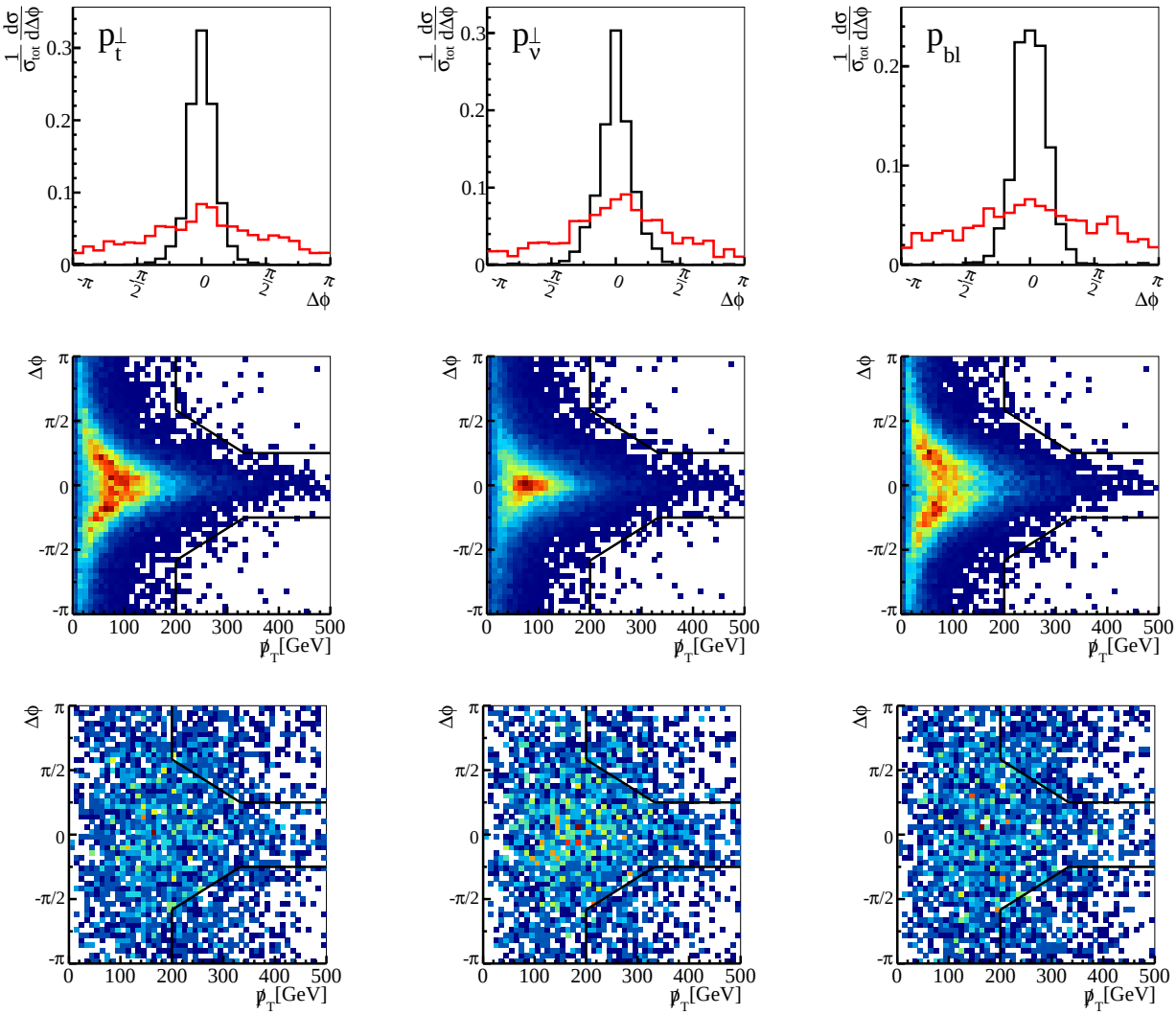

Figure 1: Top: one-dimensional $\Delta\phi$ distributions with an additional cut $\not{p}_T > 200$ GeV for the stop signal (red) and the top pair background (black). Below: two-dimensional $\not{p}_T$ vs. $\Delta\phi$ distributions for the $t\bar{t}$ background (2nd row) and for the $\tilde{t}\tilde{t}^*$ signal (3rd row). From left to right we show $\Delta\phi(\vec{\not{p}}_T, \hat{p}_{t,\ell}^{\perp})$, $\Delta\phi(\vec{\not{p}}_T, \hat{p}_{\nu}^{\perp})$ and $\Delta\phi(\vec{\not{p}}_T, \hat{p}_{b\ell})$. All plots are at the hadron level and based on the orthogonal approximation. We apply the universal selection cuts 1-5 and the border of the cut 8 is shown in the two-demensional plots.

momentum configuration we find a valid reconstructed neutrino momentum. As a consistency requirement we should check if the reconstructed neutrino momentum combined with the observed bottom and lepton momentum really corresponds to the kind of boosted top quarks which we assume to exist in the first place:

6. possible solution for respective approximation.

7. $p_{T,t}^{\text{est}} > 200$ GeV.

The orthogonal and decay plane approximations perform very differently under the first of these two requirements. By construction and as explained in the appendix, the signal efficiency of the orthogonal approximation ranges around 50% while the decay plane approximation almost always delivers a valid solution for the neutrino momentum. However, from Table II we see that this larger signal efficiency is at least compensated by the also larger background efficiency, so that in the final result the orthogonal approximation delivers a better

	orthogonal approximation							decay plane approximation						
	$\tilde{t}_1\tilde{t}_1^*$				$t\bar{t}$	W+jets	S/B	$\tilde{t}_1\tilde{t}_1^*$				$t\bar{t}$	W+jets	S/B
$m_{\tilde{t}}$[GeV]	340	440	540	640			440	340	440	540	640			440
1.-5. base cuts	27.38	13.71	6.33	2.89	642.72	2.63	0.021							
6. approximation	14.81	7.69	3.61	1.66	285.16	1.41	0.027	27.33	13.67	6.31	2.89	642.37	2.63	0.021
7. $p_T^{\rm est} > 200$GeV	8.61	4.53	2.41	1.24	215.62	0.60	0.021	9.13	5.16	2.87	1.61	242.21	0.54	0.021
8. $\not{p}_T$ vs. $\Delta\phi$ cut	0.97	1.52	1.23	0.76	0.72	0.02	2.06	1.22	1.82	1.53	1.02	1.31	0.06	1.33

Table II: Signal (for different stop masses) and backgrounds after the leptonic top tag. We show both approximations to the top momentum defined in Eq.(5). The $\not{p}_T$ vs. $\Delta\phi$ cut is defined in the text. All numbers given in fb.

signal-to-background ratio as well as a better significance for an integrated luminosity of 20 fb^{-1}. The situation might well be different for smaller luminosities where the number of signal events after all cuts becomes the main hurdle.

As the last step of our analysis, following Figure 1 we require a two-dimensional condition for the azimuthal separation defined in Eq.(7) correlated with the measured missing transverse momentum:

8. one tagged leptonic top fulfilling all three conditions

$$|\Delta\phi| > \frac{13}{12}\pi - \frac{\not{p}_T}{400\ \text{GeV}}\pi \qquad \not{p}_T > 200\ \text{GeV} \qquad |\Delta\phi| > \frac{\pi}{4}.$$

All signal and background cross sections after these signal specific cuts we show in Table II. As long as we are only interested in the direction of the leptonic top momentum but not its size the orthogonal approximation works better, which is also shown in Figure 4 in the appendix. Table III shows that over a wide range of stop masses we find of the order of 20 signal events for an integrated luminosity of 20 fb^{-1} at a collider energy of 14 TeV. The signal-to-background ratio from the orthogonal approximation ranges around $S/B \sim 1-2$ and the Gaussian significance exceeds $S/\sqrt{B} \sim 5$ for stop masses from 340 to 540 GeV. For larger stop masses the kinematics for the signal as compared to the softer continuum top pair production becomes more distinctive, so our analysis should be adapted to this parameter regime. Note that the numbers in Table III are computed at the hadron level. Applying all cuts 1.-8. gets rid of essentially all semileptonic top pair events at parton level, so the events shown as $t\bar{t}$ background in Table III are mostly mis-measured leptonic top pairs.

Also in Table III we see how the decay plane approximation performs slightly worse for the signal-to-background ratio, but gives a similar significance based on a slightly larger number of signal events after all cuts. While this significance for semileptonic stop decays might be slightly smaller than for the purely hadronic mode [6] the signal-to-background ratio is better and the efficiency of the critical hadronic top tagger is reduced to a linear dependence. Combining the two analysis strategies means that based on the order of 10 fb^{-1} of LHC data at 14 TeV (or an adjusted number for a lower collider energy) we can discover a top squark mainly decaying to top quarks and a dark matter agent in both of the two dominant top decay channels. This not only would give us faith in such an observation, it is also the starting point for detailed studies of such a new physics signal.

	orthogonal approximation				decay plane approximation			
$m_{\tilde{t}}$[GeV]	340	440	540	640	340	440	540	640
$S_{20\text{fb}^{-1}}$	19.4	30.4	24.6	15.2	24.4	36.4	30.6	20.4
S/B	1.31	2.05	1.66	1.03	0.89	1.33	1.12	0.74
$S/\sqrt{B}_{20\text{fb}^{-1}}$	5.04	7.90	6.34	3.95	4.66	6.95	5.84	3.90

Table III: Results based on the reconstructed top momentum direction for the two approximations to the neutrino momentum, Eq.(5). All eight cuts shown in Tables I and II are included. The LHC energy is 14 TeV.

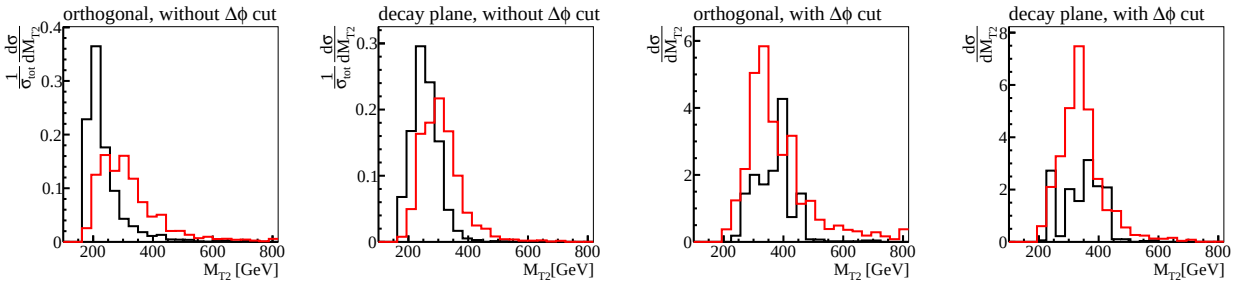

Figure 2: M_{T2} distributions for the stop signal (red) and the $t\bar{t}$ background (black). From the left we show the orthogonal and the decay plane approximations without the $\Delta\phi$ vs $\not{p}_T$ cut but with $\not{p}_T > 200$ GeV and then both of them with the $\Delta\phi$ vs $\not{p}_T$ cut. The expected endpoint is $M_{T2} < m_{\tilde{t}}(1 - m^2_{\tilde{\chi}^0_1}/m^2_{\tilde{t}}) = 418$ GeV.

III. RECONSTRUCTING THE TOP 4-MOMENTUM

The strategy described in Section II we can also use to fully reconstruct the 4-momentum of the leptonically decaying top quark. An additional question becomes how much this additional observable helps in extracting the stop signature, as compared to the results shown in Table III. Up to now the downside to our stop pair analysis is that we do not have a handle on the stop mass.

If as an additional step we want to gain more information on the heavy particle decaying into a boosted top the $M_{T,2}$ endpoint is the prime observable and requires full knowledge of the top 4-momentum [22]. As for the purely hadronic stop decay the crucial observation is that this stransverse mass endpoint to work we need a one-step stop decay into the invisible dark matter agent. A pair of top squarks decaying into tagged tops and two dark matter particles is precisely of this topology.

For the endpoint measurement, we best rely on a combination of the orthogonal and decay plane approximations. First, we use the orthogonal approximation for the basic cuts 1.-5. and the more specific top rejection cuts 6.-8. Then, we use either the orthogonal or the the decay plane approximation to compute the m_{T2} distribution, *i.e.* we define a m_{T2} variable in terms of the estimated top momenta and the estimated missing momentum from other sources than the neutrino as

$$M_{T2}\Big|_{\parallel,\perp} = M_{T2}(p^{\text{HEPTop}}_{t,h}, p^{\text{est}}_{t,\ell}, \not{p}_T - p^{\text{est}}_{T,\nu})\Big|_{\parallel,\perp} . \tag{8}$$

Once we measure the leptonic and hadronic top there should appear the endpoint

$$M_{T2} < m_{\tilde{t}} \left(1 - \frac{m^2_{\tilde{\chi}^0_1}}{m^2_{\tilde{t}}}\right) \tag{9}$$

in the stop signal events. In Figure 2 we show the M_{T2} signal and background resolutions in the orthogonal approximation and in the decay plane approximation and clearly see the signal endpoint around 418 GeV. From a purely signal point of view and without the two-dimensions $\Delta\phi$ vs. $\not{p}_T$ cut (8.) the endpoint of the stransverse mass defined in the decay plane approximation is more precise. The reason is that in the decay plane approximation the estimated top momentum is by construction almost always smaller than the true value while in the orthogonal approximation, the estimated top momentum frequently exceeds the true value, which spoils the endpoint. Note that the signal-to-background ratio S/B is still fixed by the numbers for the orthogonal approximation which we use for the event selection. This signal feature survives after we include the final $\Delta\phi$ vs. $\not{p}_T$ top rejection cut.

The top pair background at hadron level but without the two-dimensional $\Delta\phi$ vs. $\not{p}_T$ cut is slightly harder for the decay plane approximation than for the orthogonal approximation. Again, this feature generally survives the application of the $\Delta\phi$ vs. $\not{p}_T$ cut, but with a big caveat arising from the experimental resolution which should dominate the behavior of this large-M_{T2} tail. From the right two panels of Figure 2 we expect that the decay plane approximation should work slightly better after applying all base cuts and top rejection cuts,

	$\tilde{t}_1\tilde{t}_1^*$				$t\bar{t}$	W+jets	S/B	$S/\sqrt{B}_{20\text{fb}^{-1}}$
$m_{\tilde{t}}$[GeV]	340	440	540	640			440	440
1.-8. base and top rejection cuts	0.97	1.52	1.23	0.76	0.72	0.02	2.06	7.9
9. $M_{T2}\|_\parallel > 250$ GeV	0.65	1.41	1.20	0.74	0.64	0.02	2.13	7.8
$M_{T2}\|_\parallel > 350$ GeV	0.11	0.59	0.80	0.58	0.39	0.02	1.44	4.1

Table IV: Signal (for different stop masses) and backgrounds for the full stop pair analysis. All numbers given in fb.

but the final word on this comparison needs to include realistic detector effects. At this stage we rely on the orthogonal approximation to determine the direction of the top, but on the decay plane approximation for the magnitude of the top momentum.

As the final step of our stop pair analysis we need to check if the M_{T2} endpoint is useful for the actual signal extraction, *i.e.* if it improves either the significance or the signal-to-background ratio. The results of such a cut we show in Table IV. We see that the azimuthal separation of the top momentum from the missing energy vector alone is highly efficient and gets hardly improved by the additional M_{T2} cut. The only reason to consider an M_{T2} cut in the extraction of the stop signal would be to replace for example the azimuthal direction cut, which means replacing the leptonic top reconstruction of the azimuthal angle by the complete top reconstruction by our tagging algorithm. Again, this might be an option after taking into account all detector effects, but at the level of our analysis the reconstruction of the azimuthal top direction is more efficient.

IV. OUTLOOK

In this study we have corrected an earlier statement that at the LHC it is not possible to observe semileptonic stop pairs over a wide range of stop masses. In the spirit of the hadronic stop pair analysis [6] we develop a search strategy for stop pairs decaying into a boosted semileptonic top pair plus missing energy. We assume 14 TeV center of mass energy and of the order of 20 fb^{-1} of integrated luminosity. Different scenarios in collider energy and luminosity can easily be explored.

First of all, the hadronic top decay we fully reconstruct using the standard HEPTopTagger. Earlier studies of boosted leptonic top quarks [15, 16] have shown that when it comes to reconstructing the full top 4-momentum the leptonic decay is not too promising. Our approach therefore first focuses on a more limited measurement, namely the azimuthal direction of the leptonic top quark. This directional vector we can reconstruct based on a decomposition of the neutrino momentum into a leading boost direction and two orthogonal sub-leading directions. We show a detailed comparison between two different approximations and come to the conclusion that it is promising to reduce the number of kinematic unknowns in the top decay by fixing the neutrino momentum orthogonally to the lepton-bottom decay plane.

Based on this strategy we extract the stop pair signal from the dominant irreducible top pair background with 5σ significance for 20 fb^{-1} of LHC data with a signal-to-background ratio above unity for stop masses from 340 to 540 GeV. Our analysis is not optimized for any stop mass, so this result should be very generic and should be improved in particular for large stop masses. The discovery potential for semileptonic stop is of the same order as for purely hadronic stop decays, both of them based on boosted top quark reconstruction.

A full reconstruction of the top 4-momentum is considerably harder. On the other hand, to measure the stop mass for example using the classical m_{T2} endpoint we develop such a strategy. While this additional measurement has little impact on the significance or the signal-to-background ratio with which we can extract the stop signal it should allow us to determine the stop mass from an m_{T2} endpoint based on a combination of the orthogonal and decay plane approximation of the leptonic top decay.

The details of the stop mass measurement and its uncertainties need to be determined by an appropriate detector simulation. The endpoint value will give us a stop mass measurement in combination with all other supersymmetric mass measurements at the LHC. As mentioned in the introduction, the stop mass is particularly useful when we combine it with the Higgs mass because the two probe a similar set of model parameters [23].

The software used in this study will be published as part of the HEPTopTagger analysis tool [6].

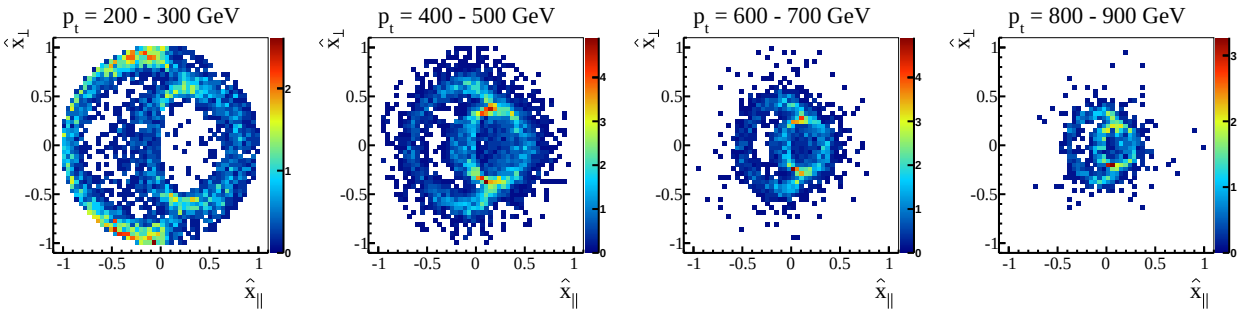

Figure 3: $(\hat{x}_\parallel, \hat{x}_\perp)$ distributions as defined in Eq.(A3) for top pair production. The four panels correspond to slices in the top momentum $200-300$ GeV, $400-500$ GeV, $600-700$ GeV, and $800-900$ GeV. All events fulfill $\not{p}_T > 150$ GeV.

Appendix A: Tagging leptonic tops

In analogy to Ref. [6] we illustrate in detail the motivation of the leptonic top tagger, its implementation, and its performance. All results shown in this appendix are based on a hadron level analysis, but without any detector simulation, just as the analysis presented in the main body of this paper. In this appendix we focus on the reconstruction of semileptonic top pairs, *i.e.* we only apply the leptonic top tagger to a sample of top pair events.

As mentioned in the main text the W and top mass conditions can be written as

$$\begin{aligned} (p_\ell + p_b + p_\nu)^2 &= m_t^2 \\ (p_\ell + p_\nu)^2 &= m_W^2 \; . \end{aligned} \tag{A1}$$

All three masses of the decay particles are known, which means that once we measure the lepton and b 4-momenta the allowed neutrino 3-momentum lies on the line which we will show can be described as the intersection of an elliptic surface and a paraboloid.

Following Eq.(3), repeated here for convenience with $\vec{p}_{b\ell} = \vec{p}_b + \vec{p}_\ell$,

$$\begin{aligned} \hat{p}^\mathrm{D} &= \frac{\vec{p}_{b\ell}}{|\vec{p}_{b\ell}|} && \text{leading } \vec{p}_{b\ell} \text{ direction in } b-\ell \text{ decay plane} \\ \hat{p}^\parallel &= \frac{\vec{p}_\ell - (\vec{p}_\ell \cdot \hat{p}^\mathrm{D})\,\hat{p}^\mathrm{D}}{|\vec{p}_\ell - (\vec{p}_\ell \cdot \hat{p}^\mathrm{D})\,\hat{p}^\mathrm{D}|} && \text{subleading direction in } b-\ell \text{ decay plane} \\ \hat{p}^\perp &= \hat{p}^\mathrm{D} \times \hat{p}^\parallel && \text{subleading direction to } b-\ell \text{ decay plane.} \end{aligned} \tag{A2}$$

we can write for example the neutrino momentum as

$$\vec{p}_\nu = x_\mathrm{D}\hat{p}^\mathrm{D} + x_\parallel \hat{p}^\parallel + x_\perp \hat{p}^\perp = p_\nu(\hat{x}_\mathrm{D}\hat{p}^\mathrm{D} + \hat{x}_\parallel \hat{p}^\parallel + \hat{x}_\perp \hat{p}^\perp) \; . \tag{A3}$$

In Figure 3 we show the two subleading $\hat{x}$ distributions for different in the originating top momentum.

In this parameterization, with $m_{b\ell}^2 = (p_\ell + p_b)^2$, the top mass constraint becomes an ellipse in three dimensions

$$\begin{aligned} &(\vec{p}_{b\ell}^{\,2} + m_{b\ell}^2)x_\parallel^2 + (\vec{p}_{b\ell}^{\,2} + m_{b\ell}^2)x_\perp^2 + m_{b\ell}^2 x_\mathrm{D}^2 - (m_t^2 - m_{b\ell}^2)|\vec{p}_{b\ell}|x_\mathrm{D} = (m_t^2 - m_{b\ell}^2)^2/4 \\ &\qquad \text{or} \qquad \frac{x_\parallel^2}{R_{t,1}^2} + \frac{x_\perp^2}{R_{t,1}^2} + \frac{(x_\mathrm{D} - \bar{x}_\mathrm{D})^2}{R_{t,2}^2} = 1 \; , \end{aligned} \tag{A4}$$

with the radii and focal point coordinate

$$R_{t,1} = \frac{m_t^2 - m_{b\ell}^2}{2m_{b\ell}} \; , \qquad R_{t,2} = \frac{\sqrt{|\vec{p}_{b\ell}|^2 + m_{b\ell}^2}}{m_{b\ell}} R_{t,1} \; , \qquad \bar{x}_\mathrm{D} = \frac{|\vec{p}_{b\ell}|}{m_{b\ell}} R_{t,1} \; . \tag{A5}$$

For the W mass constraint it is useful to define the rotated basis vectors

$$\begin{pmatrix} y_\mathrm{D} \\ y_\parallel \end{pmatrix} = \begin{pmatrix} \cos\theta_{b\ell,\ell} & \sin\theta_{b\ell,\ell} \\ -\sin\theta_{b\ell,\ell} & \cos\theta_{b\ell,\ell} \end{pmatrix} \begin{pmatrix} x_\mathrm{D} \\ x_\parallel \end{pmatrix} \ , \tag{A6}$$

using $\cos\theta_{b\ell,\ell} = \hat{p}_\ell \cdot \hat{p}^\mathrm{D}$. In these variables the W mass constraint reads

$$\begin{aligned} |\vec{p}_\ell|^2 y_\parallel^2 + |\vec{p}_\ell|^2 x_\perp^2 - m_W^2 |\vec{p}_\ell| y_\mathrm{D} &= \frac{m_W^4}{4} \\ \text{or} \qquad \frac{y_\parallel^2}{R_W^2} + \frac{x_\perp^2}{R_W^2} - \frac{2y_\mathrm{D}}{R_W} &= 1 \end{aligned} \tag{A7}$$

with the radius $R_W = m_W^2/2|\vec{p}_\ell|$.

We can now study the two approximations for the neutrino momentum defined in Eq.(5). In the decay plane approximation $x_\perp = 0$ the two mass constraints become an ellipse and a parabola in the $(x_\parallel, x_\mathrm{D})$ space

$$\frac{x_\parallel^2}{R_{t,1}^2} + \frac{(x_\mathrm{D} - \bar{x}_D)^2}{R_{t,2}^2} = 1 \qquad \text{and} \qquad \frac{y_\parallel^2}{R_W^2} - \frac{2y_\mathrm{D}}{R_W} = 1 \ . \tag{A8}$$

The neutrino momentum we obtain as the intersection of two lines, where in general there exist up to four solutions. We use the solution which gives the smallest top momentum. In the orthogonal approximation $x_\parallel = 0$ the mass conditions are the two ellipses

$$\frac{x_\perp^2}{R_{t,1}^2} + \frac{(x_\mathrm{D} - \bar{x}_D)^2}{R_{t,2}^2} = 1 \qquad \text{and} \qquad \frac{x_\perp^2}{{R'_W}^2} + \frac{(x_\mathrm{D} - \bar{x}'_D)^2}{{R''_W}^2} = 1 \ , \tag{A9}$$

with the rotated radii and focal coordinate

$$R'_W = \frac{R_W}{\sin\theta_{b\ell,\ell}}, \qquad R''_W = \frac{R_W}{\sin^2\theta_{b\ell,\ell}}, \qquad \bar{x}'_D = \frac{\cos\theta_{b\ell,\ell} R_3}{\sin^2\theta_{b\ell,\ell}} \ . \tag{A10}$$

We find these solutions for the orthogonal approximation numerically, being aware of the fact that in some cases there does not actually exist any solution. This finite efficiency we observe in our analysis results in Table II. In case we find more than one solution we keep the one which gives the smaller subtracted missing momentum $\not{p}_T - p_{T,\nu}^\mathrm{est}$.

In Figure 4 we show several measures describing the difference between the estimated leptonic top and neutrino momenta and the respective true momenta at parton level:

$$\begin{aligned} \Delta^\mathrm{est}|p_{t,\nu}| &= |p_{t,\nu}^\mathrm{est}| - |p_{t,\nu}^\mathrm{true}| \\ \Delta^\mathrm{est}\phi_{t,\nu} &= \phi_{t,\nu}^\mathrm{est} - \phi_{t,\nu}^\mathrm{true} \\ \Delta^\mathrm{est}\theta_{t,\nu} &= \theta_{t,\nu}^\mathrm{est} - \theta_{t,\nu}^\mathrm{true} \end{aligned} \tag{A11}$$

At hadron level the orthogonal approximation shown in red performs consistently better than the decay plane approximation to reconstruct the direction of the neutrino and the top momenta. We also see that the azimuthal direction of the top quark can be more precisely reconstructed than the neutrino's azimuthal direction. This occurs because compared to the bottom and lepton reconstruction the neutrino is the weak spot of the top reconstruction. This is why in our analysis described in Section II we use the top azimuthal direction estimated in the orthogonal approximation. Only considering tops with $p_{T,t} > 300$ GeV only slightly improves this picture.

If we do not apply the condition $\not{p}_T > 150$ GeV effectively on the neutrino momentum the corresponding analysis to Figure 4 paints a different picture: the decay plane approximation achieves the better resolution at parton level, and this features is largely the same at hadron level. This is the reason why our $M_{T,2}$ endpoint analysis is based on a mass reconstruction in the decay approximation (after the event selection in the orthogonal approximation).

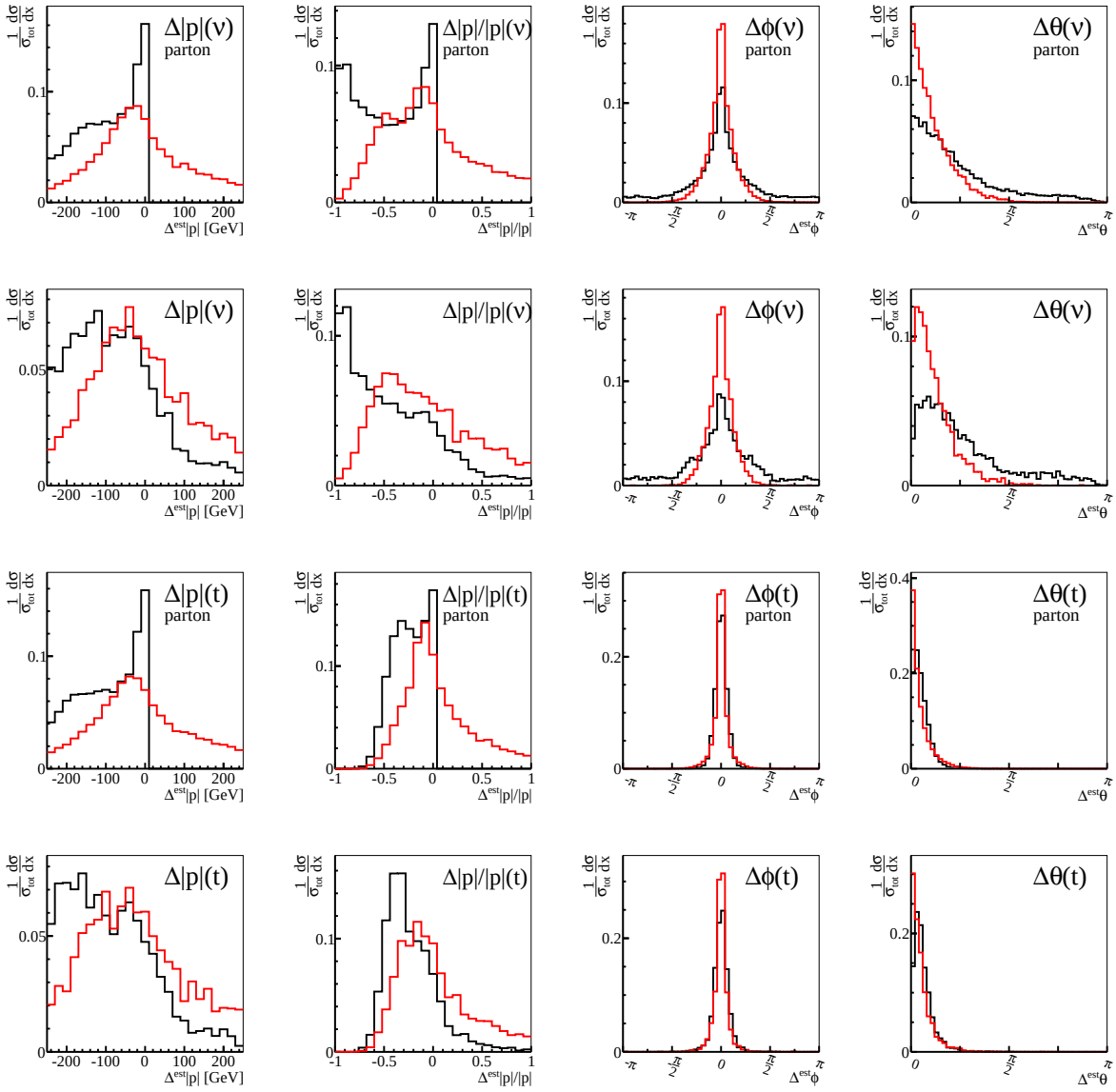

Figure 4: Absolute and relative $\Delta^{\text{est}}|p|$, $\Delta^{\text{est}}|p|/|p^{\text{true}}|$, $\Delta^{\text{est}}\phi$ and $\Delta^{\text{est}}\theta$ distributions in the decay plane approximation (black) and the orthogonal approximation (red). The upper two rows show the neutrino momentum estimate, the lower two rows the top momentum estimate. The first of the two rows is at parton level, the second row at hadron level. Only semileptonic top pair events are included. At hadron level we only require $\not{p}_T > 150$ GeV while at parton level all events also fulfill $p_{T,\ell} > 20$ GeV and $p_{T,b} > 25$ GeV.

Appendix B: Jacobian in the decay plane approximation

The relative position of the top decay products is completely determined by the vector of variables $X = (\gamma_t, \cos\theta_b, \cos\theta, \phi)$. Here, γ_t is the boost factor of the top in the laboratory frame $p_t^{\text{lab}} = \beta_t\gamma_t m_t$, θ_b is the $t \to bW$ decay angle with respect to the top direction, and (θ, ϕ) are the W decay angles in the W rest frame.

In terms of these variables, the three momenta of the decay products in the top rest frame are given by

$$p_b = \begin{pmatrix} E_b \\ 0 \\ 0 \\ |\vec{p}_b| \end{pmatrix}, \qquad p_\ell = \frac{m_W}{2} \begin{pmatrix} \gamma - \gamma\beta\cos\theta \\ \sin\theta\cos\phi \\ \sin\theta\sin\phi \\ \gamma\cos\theta - \gamma\beta \end{pmatrix}, \qquad p_\nu = \frac{m_W}{2} \begin{pmatrix} \gamma + \gamma\beta\cos\theta \\ -\sin\theta\cos\phi \\ -\sin\theta\sin\phi \\ -\gamma\cos\theta - \gamma\beta \end{pmatrix} . \tag{B1}$$

β and γ are defined by the W and b momenta in the top rest frame

$$\beta\gamma m_W = |\vec{p}_W| = |\vec{p}_b| = \frac{m_t}{2}\sqrt{1 - \left(\frac{m_W + m_b}{m_t}\right)^2}\sqrt{1 - \left(\frac{m_W - m_b}{m_t}\right)^2} , \tag{B2}$$

and $E_b = \sqrt{\vec{p}_b^{\,2} + m_b^2}$. For an unpolarized top the top decay phase space distribution in terms of the variable vector X can be written as [24]

$$P(X) = P_t(\gamma_t)\; P_W(\cos\theta) , \tag{B3}$$

where $P_t \sim \exp(-\text{const} \times \gamma_t)/\gamma_t$ is the distribution for the top momentum and P_W is the distribution for the W decay angle θ.

The problem of $P(X)$ is that it does not correspond to our measurements listed in Eq.(2). Linking the observables X to our energy measurements in the laboratory frame returns a Jacobian which dominates the distribution of the top decay products in our analysis. After boosting the lepton–bottom system by γ_t in the direction of θ_b the lepton and b energies and their invariant mass from Eq.(2) become

$$\begin{aligned} E_b^{\text{lab}} &= \gamma_t E_b + \gamma_t\beta_t |\vec{p}_b| \cos\theta_b, \\ E_\ell^{\text{lab}} &= \frac{m_W}{2}\Big[\gamma_t\gamma(1 - \beta\cos\theta) - \gamma_t\beta_t \sin\theta_b \sin\theta\sin\phi + \gamma_t\beta_t\gamma\cos\theta_b(\cos\theta - \beta)\Big], \\ m_{b\ell}^2 &= \frac{m_t^2 - m_W^2 + m_b^2}{2} - m_t|\vec{p}_b|\cos\theta , \end{aligned} \tag{B4}$$

These observables we can express in terms of dimensionless vector $Y = (\gamma_t, \tilde{E}_b, \tilde{E}_\ell, \tilde{m}_{b\ell}^2)$ including

$$\tilde{E}_b = \frac{E_b^{\text{lab}}}{|\vec{p}_b|}, \qquad \tilde{E}_\ell = 2\frac{E_\ell}{m_W}, \qquad \tilde{m}_{b\ell}^2 = \frac{m_{b\ell}^2}{m_t|\vec{p}_b|} . \tag{B5}$$

Using the relation $P(X)dX = P_Y(Y)dY$, the distribution $P_Y(Y)$ after a variable transformation can be calculated from the identity

$$\begin{aligned} P_Y(Y) &= \det\left|\frac{\partial Y}{\partial X}\right|^{-1} \; P_t(\gamma_t)\; P_W\left(\frac{m_t^2 - m_W^2 + m_b^2}{2m_t|\vec{p}_b|} - \tilde{m}_{b\ell}^2\right) \\ \text{with} \quad \det\left|\frac{\partial Y}{\partial X}\right| &= \gamma_t^2\,\beta_t^2\,\sin\theta_b\,\sin\theta\,|\cos\phi| = \gamma_t\beta_t\sqrt{A\gamma_t^2 + 2B\gamma_t + C} , \end{aligned} \tag{B6}$$

in terms of θ given by the last line of Eq.(B4) and

$$\begin{aligned} A &= -\sin^2\theta\,\left(\frac{E_b^2}{|\vec{p}_b|^2} - 1\right) - \gamma^2\sin^4\theta\,(1+\beta)^2 \\ B &= \sin^2\theta\,\frac{\tilde{E}_b E_b}{|\vec{p}_b|} - \gamma\sin^2\theta\,(1+\beta)\,[\tilde{E}_\ell - \gamma(\cos\theta - \beta)\tilde{E}_b] \\ C &= -\sin^2\theta\,(1 + \tilde{E}_b^2) - [\tilde{E}_\ell - \gamma(\cos\theta - \beta)\tilde{E}_b]^2, \end{aligned} \tag{B7}$$

Once we measure the Y components $(\tilde{E}_b, \tilde{E}_\ell, \tilde{m}_{b\ell})$ we can estimate the top momentum according to this probability $P_Y(Y)$. The poles in the Jacobian $\det|\partial Y/\partial X| = 0$ give us a pronounced Jacobian peak and constrain the

allowed range of the top momentum. Following Eq.(B6) the peak position implies $\cos\phi = 0$, which corresponds to the kinematic configuration where $\vec{p}_b$, $\vec{p}_\ell$ and $\vec{p}_\nu$ are coplanar.

Moreover, the pole condition is a quadratic equation for γ_t which has two solutions. Because $P_t(\gamma_t)$ is steeply falling for increasing γ_t the most likely value for γ_t is the smaller one. To estimate the top quark momentum we therefore choose the solution which yields the smaller momentum in the decay plane approximation ($x_\perp = 0$).

[1] D. E. Morrissey, T. Plehn and T. M. P. Tait, arXiv:0912.3259 [hep-ph].

[2] P. Meade and M. Reece, Phys. Rev. D **74**, 015010 (2006).

[3] A. Djouadi, W. Hollik and C. Jünger, Phys. Rev. D **54**, 5629 (1996); S. Kraml, H. Eberl, A. Bartl, W. Majerotto and W. Porod, Phys. Lett. B **386**, 175 (1996); W. Beenakker, R. Höpker, T. Plehn and P. M. Zerwas, Z. Phys. C **75**, 349 (1997).

[4] T. Aaltonen *et al.* [CDF Collaboration], CDF Note 9834, 2009; V. M. Abazov *et al.* [D0 Collaboration], Phys. Lett. B **665**, 1 (2008).

[5] T. Aaltonen *et al.* [CDF Collaboration], arXiv:0912.1308 [hep-ex]; V. M. Abazov *et al.* [D0 Collaboration], Phys. Lett. B **675**, 289 (2009).

[6] T. Plehn, M. Spannowsky, M. Takeuchi, and D. Zerwas, JHEP **1010**, 078 (2010); `http://www.thphys.uni-heidelberg.de/~plehn/HepTopTAGGER/`

[7] J. Ellis, F. Moortgat, G. Moortgat-Pick, J. M. Smillie and J. Tattersall, Eur. Phys. J. C **60**, 633 (2009); K. Rolbiecki, J. Tattersall and G. Moortgat-Pick, arXiv:0909.3196 [hep-ph]; M. Perelstein and A. Weiler, JHEP **0903**, 141 (2009).

[8] W. Skiba and D. Tucker-Smith, Phys. Rev. D **75**, 115010 (2007); B. Holdom, JHEP **0703**, 063 (2007). K. Agashe, A. Belyaev, T. Krupovnickas, G. Perez and J. Virzi, Phys. Rev. D **77**, 015003 (2008); M. Gerbush, T. J. Khoo, D. J. Phalen, A. Pierce and D. Tucker-Smith, Phys. Rev. D **77**, 095003 (2008); D. E. Kaplan, K. Rehermann, M. D. Schwartz and B. Tweedie, Phys. Rev. Lett. **101**, 142001 (2008); G. Brooijmans, ATL-PHYS-CONF-2008-008 and ATL-COM-PHYS-2008-001, Feb. 2008 L. G. Almeida, S. J. Lee, G. Perez, G. Sterman, I. Sung and J. Virzi, Phys. Rev. D **79**, 074017 (2009); L. G. Almeida, S. J. Lee, G. Perez, I. Sung and J. Virzi, Phys. Rev. D **79**, 074012 (2009); D. Krohn, J. Thaler and L. T. Wang, arXiv:0903.0392 [hep-ph]; for a recent overview see *e.g.* A. Abdesselam, E. B. Kuutmann, U. Bitenc *et al.*, [arXiv:1012.5412 [hep-ph]].

[9] T. Plehn, G. P. Salam and M. Spannowsky, Phys. Rev. Lett. **104**, 111801 (2010).

[10] M. H. Seymour, Z. Phys. C **62**, 127 (1994); J. M. Butterworth, B. E. Cox and J. R. Forshaw, Phys. Rev. D **65**, 096014 (2002); J. Thaler, K. Van Tilburg, [arXiv:1011.2268 [hep-ph]]; Y. Cui, Z. Han, M. D. Schwartz, [arXiv:1012.2077 [hep-ph]].

[11] S. D. Ellis, C. K. Vermilion and J. R. Walsh, arXiv:0903.5081 [hep-ph] and arXiv:0912.0033 [hep-ph]; C. K. Vermilion, [arXiv:1101.1335 [hep-ph]].

[12] J. M. Butterworth, A. R. Davison, M. Rubin and G. P. Salam, Phys. Rev. Lett. **100**, 242001 (2008); ATLAS note, ATL-PHYS-PUB-2009-088; D. E. Soper and M. Spannowsky, arXiv:1005.0417 [hep-ph]; C. R. Chen, M. M. Nojiri and W. Sreethawong, arXiv:1006.1151 [hep-ph]; A. Falkowski, D. Krohn, J. Shelton, A. Thalapillil and L. T. Wang, arXiv:1006.1650 [hep-ph]; C. Hackstein, M. Spannowsky, Phys. Rev. **D82**, 113012 (2010); C. Englert, C. Hackstein, M. Spannowsky, Phys. Rev. **D82**, 114024 (2010); K. Black, J. Gallicchio, J. Huth *et al.*, [arXiv:1010.3698 [hep-ph]]; J. -H. Kim, [arXiv:1011.1493 [hep-ph]].

[13] J. M. Butterworth, J. R. Ellis and A. R. Raklev, JHEP **0705**, 033 (2007); J. M. Butterworth, J. R. Ellis, A. R. Raklev and G. P. Salam, arXiv:0906.0728 [hep-ph]; C. S. Cowden, S. T. French, J. A. Frost and C. G. Lester [The ATLAS Collaboration], ATLAS-PHYS-PUB-2009-076, June 2009; G. D. Kribs, A. Martin, T. S. Roy and M. Spannowsky, arXiv:0912.4731 [hep-ph] and arXiv:1006.1656 [hep-ph]; G. D. Kribs, A. Martin, T. S. Roy, [arXiv:1012.2866 [hep-ph]].

[14] see *e.g.* V. Barger, T. Han and D. G. E. Walker, Phys. Rev. Lett. **100**, 031801 (2008); U. Baur and L. H. Orr, Phys. Rev. D **76**, 094012 (2007); T. Han, R. Mahbubani, D. G. E. Walker and L. T. E. Wang, JHEP **0905**, 117 (2009).

[15] J. Thaler and L. T. Wang, JHEP **0807**, 092 (2008).

[16] K. Rehermann, B. Tweedie, [arXiv:1007.2221 [hep-ph]].

[17] M. Cacciari and G. P. Salam, Phys. Lett. B **641**, 57 (2006); M. Cacciari, G. P. Salam and G. Soyez, `http://fastjet.fr`

[18] G. Corcella *et al.*, arXiv:hep-ph/0210213; M. Bahr *et al* , arXiv:0812.0529 [hep-ph].

[19] W. Beenakker, M. Krämer, T. Plehn, M. Spira and P. M. Zerwas, Nucl. Phys. B **515**, 3 (1998).

[20] P. Nason, S. Dawson and R. K. Ellis, Nucl. Phys. B **303**, 607 (1988); W. Beenakker, H. Kuijf, W. L. van Neerven and J. Smith, Phys. Rev. D **40**, 54 (1989); S. Moch and P. Uwer, Phys. Rev. D **78**, 034003 (2008).

[21] M. L. Mangano, M. Moretti, F. Piccinini, R. Pittau and A. D. Polosa, JHEP **0307**, 001 (2003).

[22] C. G. Lester and D. J. Summers, Phys. Lett. B **463**, 99 (1999); A. Barr, C. Lester and P. Stephens, J. Phys. G **29**,

2343 (2003).
[23] R. Lafaye, T. Plehn, M. Rauch and D. Zerwas, Eur. Phys. J. C **54**, 617 (2008); P. Bechtle, K. Desch, M. Uhlenbrock and P. Wienemann, [arXiv:0907.2589 [hep-ph]].
[24] G. L. Kane, G. A. Ladinsky and C. P. Yuan, Phys. Rev. D **45**, 124 (1992).